Cross-binding of Four Adenosine/ATP Aptamers to Caffeine, Theophylline and Other Methylxanthines

Yuzhe Ding[a§], Yachen Xie[a§], Albert Zehan Li[a], Po-Jung Jimmy Huang[a] and Juewen Liu[a*]

[a] Department of Chemistry, Waterloo Institute for Nanotechnology, University of Waterloo, Waterloo, ON, N2L 3G1, Canada

[§] Y. Ding and Y. Xie contributed equally to this work.

*Email: liujw@uwaterloo.ca

Abstract

The classical DNA aptamer for adenosine and ATP was selected twice using ATP as the target in 1995 and 2005, respectively. In 2022, this motif appeared four more times from selections using adenosine, ATP, theophylline and caffeine as targets, respectively, suggesting that this aptamer can also bind methylxanthines. In this work, using thioflavin T fluorescence spectroscopy, this classical DNA aptamer showed K_d values for adenosine, theophylline and caffeine of 9.5, 101 and 131 μM, respectively, and similar K_d values were obtained using isothermal titration calorimetry. Binding to the methylxanthines was also observed for the newly selected Ade1301 aptamer, but the Ade1304 aptamer. The RNA aptamer for ATP also had no binding to the methylxanthines. Molecular dynamics simulations were performed using the classical DNA and RNA aptamers based on their NMR structures, and the simulation results were consistent with the experimental observations, explaining the selectivity profiles. This study suggests that a broader range of target analogs need to be tested for aptamers. For the detection of adenosine and ATP, the Ade1304 aptamer is a better choice due to its better selectivity.

Introduction

ATP-binding aptamers have been critical for the development of the aptamer field.[1] The Szostak lab reported an RNA aptamer in 1993 with a K_d of 0.7 μM ATP.[2] The same lab also reported a DNA aptamer in 1995,[3] which can bind ATP, AMP and adenosine (K_d around 6 μM adenosine, no binding to G, C or U).[3,4] These aptamers were obtained using an ATP column. Interestingly the same DNA aptamer was also selected by Nutiu and Li using a library immobilization method in 2005.[5] This classical DNA aptamer has been used not only for the development of biosensors,[1,6-12] but also for fundamental biochemical studies.[13-15] Based on NMR spectroscopy and isothermal titration calorimetry (ITC), this DNA aptamer binds two target molecules.[4,16-18] Each target molecule forms hydrogen bonds with a guanine and stacks with other bases.[16]

By immobilizing a DNA library that can fold to a hairpin structure,[19-21] we recently used adenosine and ATP as targets and also observed this classical aptamer in the early rounds of the selections when the target concentrations were high.[22] In the late rounds, when the target concentrations were dropped to as low as 1 μM, this sequence was suppressed and two higher affinity aptamers (K_d ~200 nM adenosine) dominated.

The other branch of purine-binding aptamers focused on theophylline,[23] and the RNA aptamer for theophylline is the most cited example for highlighting the selectivity of aptamers.[24] We also performed aptamer selections using methylxanthines such as caffeine and theophylline as targets.[25,26] The selected aptamers had K_d values in the range of 0.5 to 3 μM for their respective target. Interestingly, the classical adenosine DNA aptamer also appeared in these selections,[27] suggesting its binding to methylxanthines. Herein, we studied their binding using fluorescence spectroscopy and isothermal titration calorimetry (ITC). In addition, we also studied the two newly selected DNA aptamers along with the RNA aptamer for ATP. Based on the selectivity profiles, we believe at least two types of binding sites exist. The selectivity was also rationalized using molecular dynamics simulations.

Materials and Methods

Chemicals. The DNA samples used for selection and sensing were purchased from Integrated DNA Technologies (Coralville, IA, USA). The sequence details are listed in Table S1. Caffeine, theophylline, theobromine, paraxanthine, adenosine, adenine, guanine, xanthine, 2-aminopurine, GMP, ThT, and magnesium chloride were purchased from Millipore-Sigma (Oakville, ON, Canada). 4-(2-Hydroxyethyl)piperazine-1-ethanesulfonic acid (HEPES) and its sodium salt form were from Biobasic Inc. (Markham, ON, Canada). All buffers and solutions were prepared with

Milli-Q water. In vitro transcription was performed using a kit from New England Biolabs (HiScribe® T7 Quick High Yield RNA Synthesis Kit).

ThT fluorescence spectroscopy. For a typical experiment, 100 nM aptamer and 2 μM ThT were dissolved in 10 mM HEPES buffer, pH 7.6 with 50 mM NaCl, 4 mM Mg^{2+}. Different concentrations of target were titrated and the fluorescence was monitored in a Horiba Fluoromax 4 fluorometer with excitation at 420 nm and emission at 490 nm. The temperature was set at 20°C using a water bath. The fluorescence was equilibrated to reach a stable value before titration was performed. For calculation of K_d values, the fluorescence intensity was corrected by considering dilution due to added target molecules, and the data were fitted using $F = F_0 - A[C]/(K_d + [C])$, where F is the fluorescence measured at a given target concentration $[C]$, F_0 is the initial fluorescence before adding the target, and A is the maximal fluorescence drop.

ITC. ITC was performed using a MicroCal VP-ITC instrument as described previously.[22] DNA (20 or 50 μM, 2 mL) and target molecules (1 mM or 3.5 mM, 2 mL) were dissolved in buffer (20 mM HEPES, 50 mM NaCl and 4 mM $MgCl_2$) and degassed for 10 min prior to measurement. A volume of 1.4 mL aptamer was loaded into the cell chamber and 300 μL target was loaded in the syringe. Except for an initial injection of 0.5 μL, 10 μL of target was titrated into the cell each time over 20 sec duration for a total of 20 injections at 25°C. The spacing was set for 360 sec between each injection. The thermodynamic values were obtained by fitting the titration curves to a one-site binding model using the Origin software.

Molecular dynamics (MD) simulations. The initial coordinate of the aptamers was prepared based on the NMR structure (PDB ID: 1AW4 and 1RAW).[16,28] To assess the aptamers and different ligands, we replaced an AMP (binding with G_9 for the DNA aptamer) in the initial aptamer complex to adenine, caffeine, or guanine, respectively, by the Pymol program. For the RNA aptamer, the same replacement was performed. The only difference was that the simulation time of equilibrium dynamics was extended as the RNA appeared to be more flexible than the DNA. Each aptamer complex was simulated by the same MD cascade as described below. The aptamer complex was solvated in a water box (TIP3 model) using the VMD program.[29] The smallest distance between the aptamer complex, and the faces of the periodic cubic water box was 10 Å. Besides, the aptamer complex system was neutralized by 0.1 M NaCl and 0.005 M $MgCl_2$ to imitate the experiment environment. Then, this system was energy minimized, equilibrated and produced using the NAMD program[30] with the all-atom CHARMM36 nucleic acid force field, CGenFF force field, and SwissParam online system.[31-33]

In all MD cascades, bonds to all hydrogen atoms were constrained by the SHAKE algorithm,[34] and the time step was 2 fs. The system was simulated in periodic boundary

conditions, with full electrostatics computed using the PME method[35] with grid spacing on the order of 1 Å or less. Short-range nonbonded terms were evaluated every step using a 12 Å cut-off for van der Waals interactions and a smooth switching function. First, each system was minimized with fixed positions of the aptamer complex for 1000 steps of conjugate gradient. Then, a 100 ps heating process from 0 to 368 K and a 100 ps cooling process from 368 K to 298 K in a canonical ensemble (NVT) were performed. Lastly, production dynamics was performed at isothermal-isobaric ensemble (NPT). The temperature was maintained at 298 K using weakly coupled Langevin dynamics of non-hydrogen atoms,[36] and the pressure was 1 atm and maintained by the Langevin piston Nosé-Hoover method.[37] The production dynamics of DNA complex was at least 1 ns and that of the RNA complex was at least 3 ns. All of the MD data were based on the MD trajectory of production dynamics.

Results and Discussion

The classical adenosine aptamer binds caffeine and theophylline

The secondary structure of the classical adenosine aptamer is shown in Figure 1A, and the two target molecules are represented by the red A symbols.[16] The structure of adenosine and some other purine derivatives are shown in Figure 1B. Each adenosine forms two hydrogen bonds with an unpaired guanine (G_9 or G_{22}). In addition, the G·A mismatched pairs are stacked with other purines on both sides. We also discovered this aptamer motif from the early rounds of our caffeine and theophylline selections,[27] and its abundance reached 50% in the round 15 caffeine selection library (Figure S1).

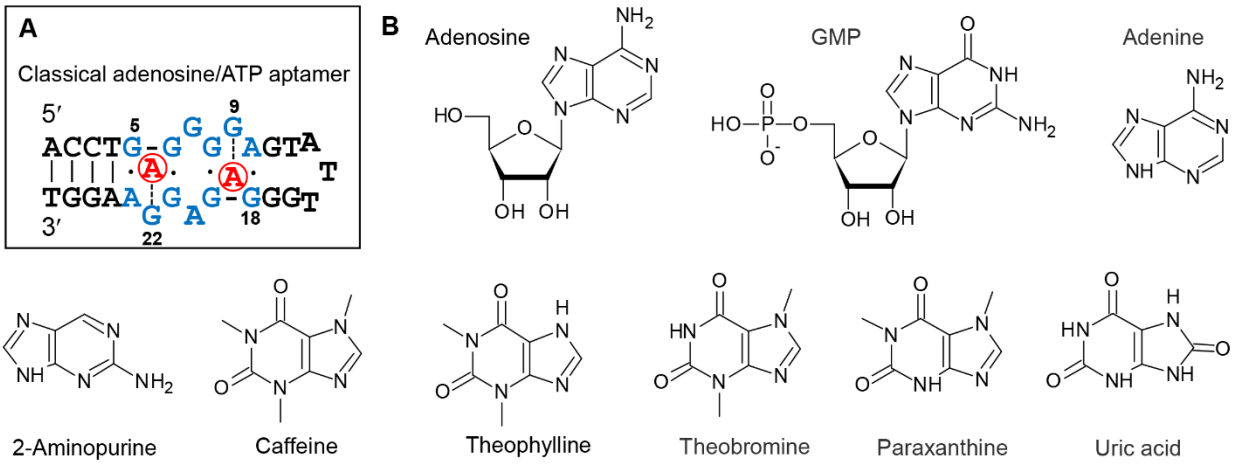

Figure 1. (A) The secondary structure of the classical adenosine/ATP aptamer. (B) The structures of some purine derivatives used in this study.

The guanine-rich conserved regions allowed us to use thioflavin T (ThT) as a probe to study aptamer binding.[38-40] Free ThT is almost nonfluorescent, but its fluorescence is enhanced upon binding to guanine-rich DNA. Aptamer binding to its target may displace ThT, leading to decreased fluorescence (Figure 2A). After binding to the adenosine aptamer, ThT showed a fluorescence peak at 490 nm, which dropped by 50% upon adding 200 μM adenosine (Figure 2B). From this titration, we obtained a binding curve with a fitted K_d of 9.5 μM adenosine (Figure 2C, black trace), which is comparable with literature reports.[3,17,41] Using this method, we also observed binding with theophylline (K_d 101 μM), caffeine (~130 μM) and theobromine (~130 μM), although paraxanthine showed a significantly higher K_d of 628 μM. Therefore, this adenosine aptamer binds all these methylxanthines.

We then test a few other adenosine analogs including adenine and 2-aminopurine (Figure 2D). A K_d of 30 μM adenine was obtained, which was consistent with the literature that adenosine binds more strongly than adenine to this aptamer.[3] 2-Aminopurine showed even weaker binding (K_d = 151 μM). Moving the amine group from the 6′ position to 2′ position disrupted the original hydrogen bonding pattern, explaining the weakened binding affinity to 2-aminopurine. Finally, we tested uric acid and GMP, which showed almost no binding (Figure 2E). For these two compounds, an accurate fitting of K_d cannot be obtained. We did not test guanine or guanosine due to their poor solubility but used GMP instead. Therefore, among these molecules, the ranking of binding affinity is adenosine > caffeine, theophylline, theobromine, 2-aminopuine > paraxanthine > uric acid, GMP. Previous studies on this aptamer focused on the comparison with G, T/U, and C nucleosides/nucleotides.[3,41,42] To our knowledge, this is the first measurement of its binding to methylxanthines.

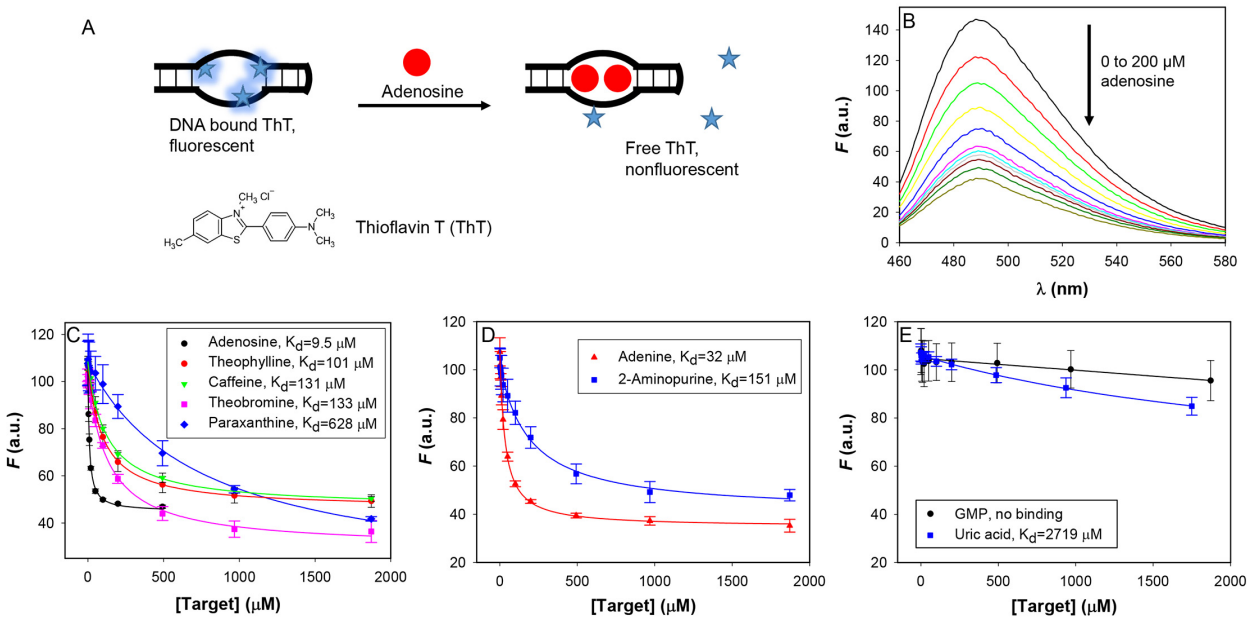

Figure 2. (A) A scheme of the ThT-based fluorescent binding assay. (B) Fluorescence spectra of ThT with the classical aptamer in the presence of various concentration of adenosine in 50 mM NaCl, 4 mM $MgCl_2$ and 10 mM HEPES, pH 7.5. The quenched fluorescence can be used for label-free binding assays. ThT-based assay of the binding of the classical aptamer to (C) adenosine, caffeine, theophylline, theobromine, and paraxanthine; (D) adenine and 2-aminopurine; and (E) uric acid and GMP.

ITC characterization of binding

To confirm the ThT assay results and obtain quantitative binding thermodynamic values, we then performed isothermal titration calorimetry (ITC).[43] Adenosine titration showed a K_d of 8.2 μM (Figure 3A), consistent with the ThT assay. We then performed ITC by titrating theophylline and caffeine. The K_d for caffeine was 62 μM (Figure 3B), and for theophylline was 64 μM (Figure 3C). These K_d values were just around 8-fold higher than that for the binding of adenosine. The *c*-values (N·[aptamer]/K_d) of these ITC experiments were close to 2 and all the titrations reached saturation, and thus the fitting quality should be reliable.[44]

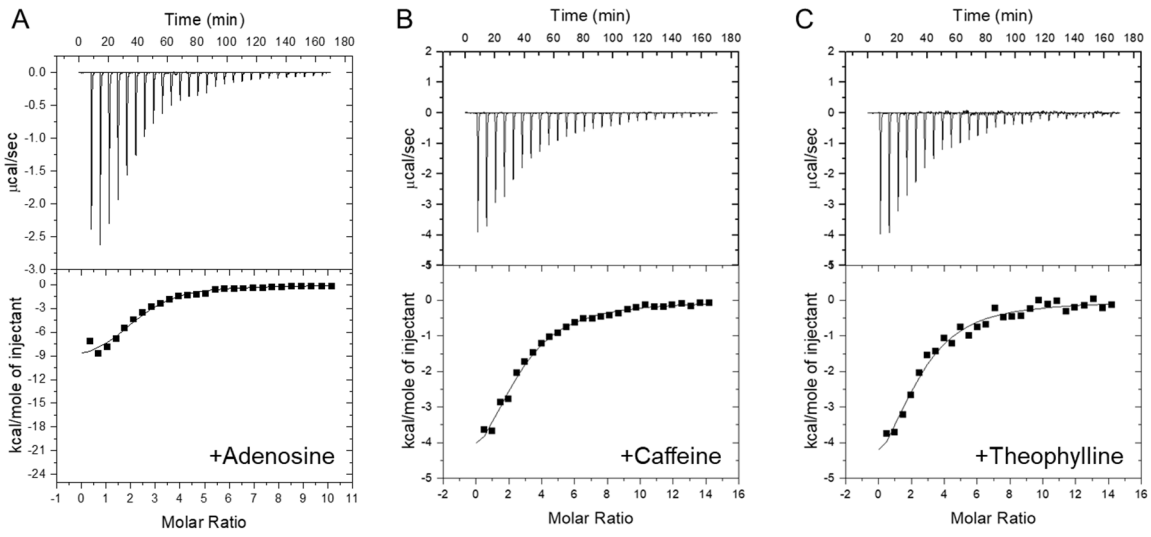

Figure 3. ITC traces and the integrated heat of titrating (A) 1 mM adenosine into 20 µM classical aptamer; (B) 3.5 mM caffeine and (C) 3.5 mM theophylline into 50 µM classical aptamer. The buffer contained 50 mM NaCl and 4 mM $MgCl_2$. Panel (A) adapted from Ref.[22] with permission. Copyright 2023 American Chemical Society.

Table 1. The thermodynamic values of the classical DNA aptamer binding to adenosine, caffeine and theophylline.

Target	***N***	**Δ*H* (kcal/mol)**	**Δ*S* (cal/K·mol)**	**K_d (µM)**
Adenosine	2.3	-10.2 ± 0.7	-11	8.2 ± 1.7
Caffeine	2.5	-6.0 ± 0.5	-0.9	62 ± 8
Theophylline	2.3	-6.5 ± 0.9	-2.7	64 ± 14

Methylxanthines bind in the same pocket as adenosine

An interesting question is whether the methylxanthines bind to the same sites as adenosine or they simply nonspecifically bind to the aptamer at other sites. We tend to believe the former for the following reasons. First, the same aptamer motif was obtained by using caffeine and theophylline as target for aptamer selection,[27] suggesting that they are functionally equivalent to adenosine for binding to this aptamer. Second, we noted that all the tested targets had a binding stoichiometry *N* close to 2 (Table 1), meaning each aptamer binds to two target molecules. Since an *N* of 2 is a unique feature of the classical adenosine aptamer, we reasoned that all these

targets were bound to a similar overall structure of the aptamer simply by replacing adenosine with caffeine or other methyxanthines.

To further confirm our hypothesis, we designed a G9A and G22A double mutant, and this should disrupt adenosine binding, but its perturbation to nonspecific binding might be minimal. We used ThT to monitor binding and both adenosine and caffeine showed K_d values greater than 500 μM (Figure S2), suggesting that caffeine binding to the wild-type aptamer was specific.

Selectivity of the two new DNA aptamers

We recently selected two new DNA aptamers, both with around 200 nM affinity for adenosine.[22] An interesting question is whether they can bind to methylxanthines. The structure of the Ade1301 aptamer is shown in Figure 4A, and the conserved nucleotides are shown in red. When adenosine was titrated, the ThT fluorescence dropped about 80% making it a useful binding assay (Figure 4C, the red line). The fitted K_d was 0.76 μM adenosine under the experimental condition. The previously measured K_d using ITC was 0.23 μM, and this small difference could be due to buffer condition (e.g. 4 mM Mg^{2+} here versus 20 mM Mg^{2+} in the ITC).

We then used the ThT fluorescence to measure the binding of other purine analogs. All the tested methylxanthines can bind to Ade1301 with K_d mostly around 10 to 20 μM. This was around 20-fold higher than its binding of adenosine. Ade1301 and the classical DNA aptamer have very different binding sequences and stoichiometry, but they have a similar selectivity profile.

The structure of the Ade1304 aptamer is shown in Figure 4B.[22] We then tested Ade1304 using the ThT method, and adenosine caused a 90% fluorescence drop with a K_d of 0.99 μM. Surprisingly, Ade1304 has much better selectivity with little binding to the methylxanthines (Figure 4D). Among the tested molecules, only adenine showed a weak binding with a K_d of 225 μM.

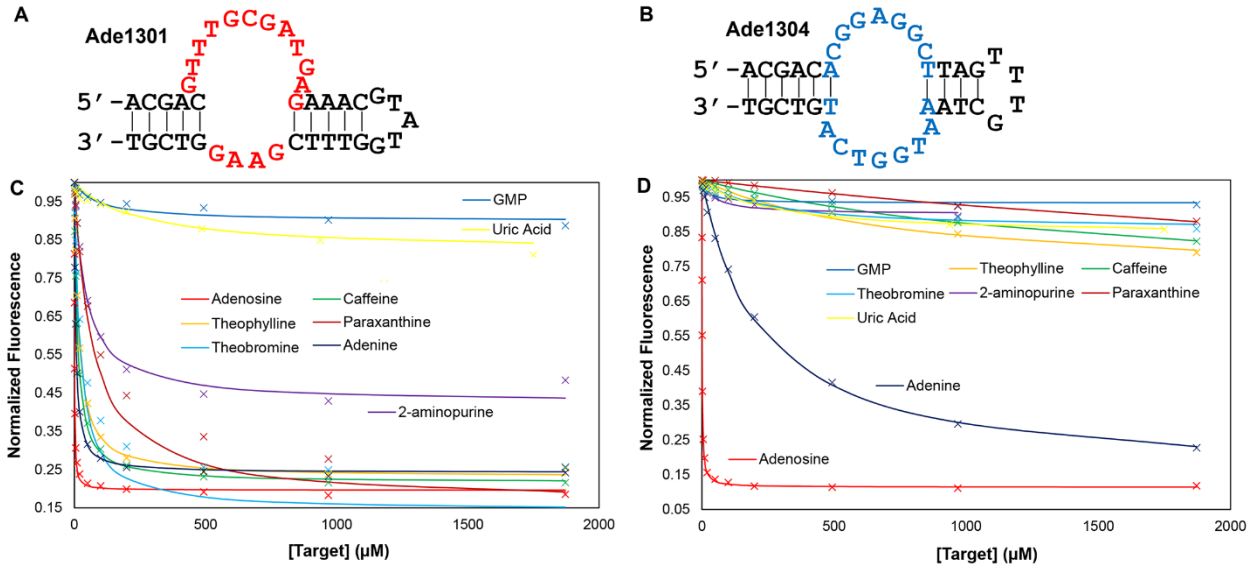

Figure 4. Structure of the (A) Ade1301 and (B) Ade1304 aptamers. The drop of ThT fluorescence for the (C) Ade1301 and (D) Ade1304 aptamers upon titration of various concentration of purine derivatives. The experiments were run with 100 nM aptamer and 2 μM ThT in 10 mM HEPES buffer, pH 7.6 with 50 mM NaCl, 4 mM $MgCl_2$. Each titration was run in triplicate and the average values are plotted here.

We plotted the fitted K_d values for these three aptamers in Figure 5, where the relative positions of the black and red bars are similar for all these molecules, except that the black bars are always higher. This observation quantitatively indicates a binding similarity between the classical aptamer and Ade1301. The selectivity of Ade1304 is obviously higher. Therefore, for biosensor applications, Ade1304 is a more specific probe for the detection of adenosine and ATP.

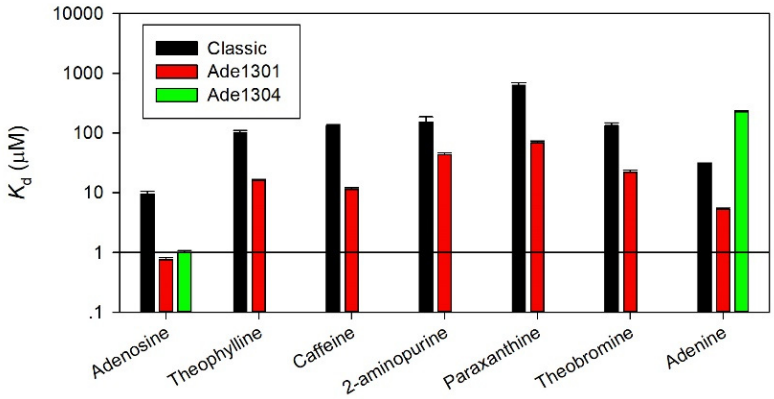

Figure 5. The K_d values of the three DNA aptamers. Data for uric acid and GMP are excluded since they cannot be accurately fitted, and the estimated K_d values for them are larger than 1 mM. For the positions without a green bar, it also means binding was too weak to fit.

MD simulations to understand selectivity

Based on the above data, at least two types of adenosine binding pockets exist. One is highly specific, whereas the other can bind to methylxanthines with around 20-fold lower affinities than adenosine. To rationalize the binding specificity, we used MD simulation. We first studied the classical DNA aptamer, since its NMR structure is available.[16] We classified target analytes into three types based on binding affinity. The first type is the adenosine derivatives, which have a high binding affinity (K_d ~6 to 30 μM). The second type includes caffeine, theophylline and other methylxanthines with K_d higher than 100 μM. The final class is guanine derivatives and uric acid, which do not bind.

For the first type, we chose adenine as the ligand. Based on the NMR structure,[16] the exocyclic amine group of the adenine ligand is a hydrogen bond (HB) donor and the N1 nitrogen is a HB acceptor, forming two HBs to an unpaired guanine (Figure 6A). In addition, π-π stacking occurs with the topic and bottom bases.[16] Based on a previous simulation work, this binding structure collapsed when just HBs are formed.[14] For the MD simulation, we started with an adenine in the NMR structure of the aptamer (only one of the two binding sites was simulated), and allowed the system to achieve a dynamic equilibrium. We sampled 500 conformations evenly from 1 ns MD trajectory of equilibration, which revealed that the binding structure remained (Figure 6A), and these two HBs were formed stably. From their time-dependent bond length change (Figure 6B), the average lengths of HB1 and HB2 are 2.3±0.4Å and 2.0±0.3Å,

respectively. The small change (HB1 17% and HB2 15%) in the bond length is consistent with the harmonic vibrations of bonds expected for a stable binding structure.

To understand binding of methylxanthines, we inserted a caffeine based on the lowest binding energy conformation suggested by docking. After the same procedures as above, caffeine and the aptamer also formed two HBs (Figure 6C). The way of caffeine binding can also explain the binding of other methylxanthines since the three methyl groups are not involved in HB. As shown in Figure 6D, the average length of HB1 is 2.8±0.9 Å and the average length of HB2 is 2.2±0.5 Å. The longer bonds indicated that the strength of these HBs was weaker than that with adenine (i.e. shorter HBs are more stable). In addition, the bond lengths showed much larger variations as a function of time (HB1 32% and HB2 23%) compared to that for adenine (Figure 6B), suggesting that the HBs were less stable.

Finally, we tested guanine as a negative control. The standard MD process shows that guanine cannot form strong molecule interactions with the aptamer because only one HB was formed with the aptamer at the beginning of the simulation (Figure 6E). Then, this HB breaks over time, leading to the dissociation of guanine from the aptamer as evident from the large distance increase at the end of the simulation (Figure 6F). Therefore, the MD simulation results are consistent with the experimental observations, and the affinity of target binding can be rationalized from the aptamer structure.

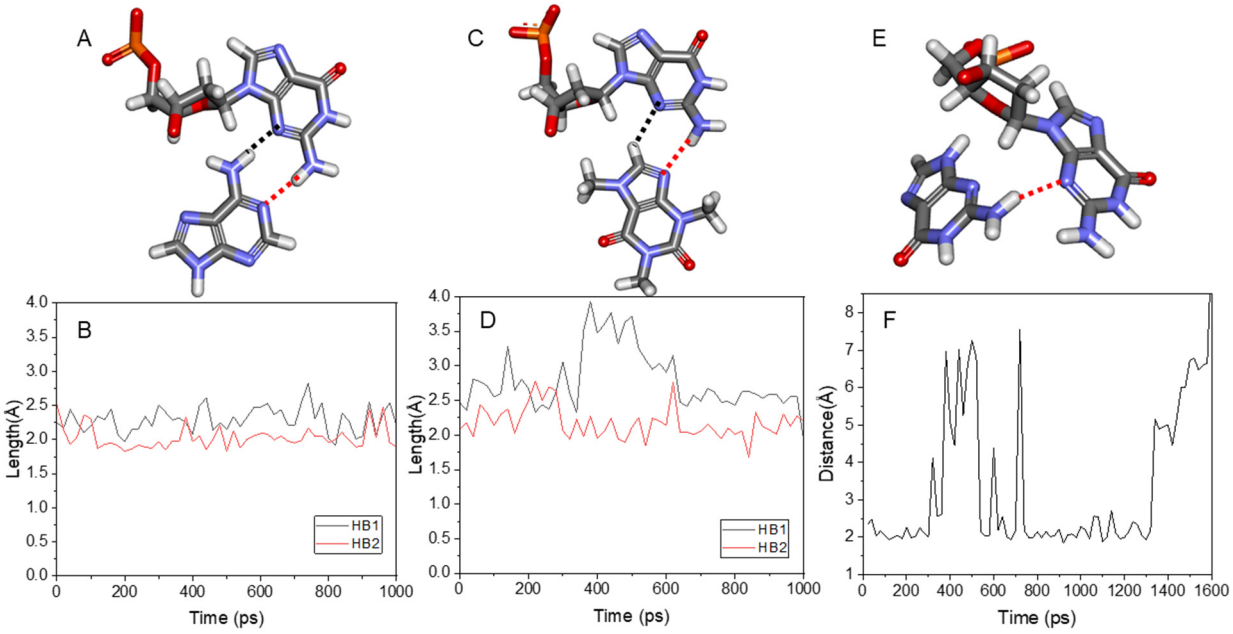

Figure 6. (A) The MD simulated equilibrium binding structure of G_9 in the classical adenosine aptamer using adenine as the target ligand, and this structure is consistent with the NMR structure. (B) The bond lengths of the two HBs formed between G_9 and adenine. (C) The binding

structure of G9 and caffeine. (D) The length of the HBs between G_9 and caffeine. (E) The binding structure of G9 and guanine. (F) The length of the HB between G_9 and guanine.

5. The RNA aptamer is highly selective

We then studied the RNA aptamer for ATP.[2] Based on its NMR structure, this RNA aptamer (Figure 7A) has seven bases to interact with an AMP ligand.[28,45] The AMP forms HB with G_8, A_{12}, U_{16}, G_{17} and G_{30} respectively, and π-π stacks with A_{10} and G_{11}. We in vitro transcribed the RNA aptamer. Using the ThT assays, adenosine showed a K_d of 2.8 μM (Figure 7B). This value (collected with 4 mM Mg^{2+}) is comparable to that reported in the original paper by Szostak (1.7 to 2.7 μM).[2] Importantly, theophylline and caffeine showed no fluorescence change, indicating a lack of binding with these methylxanthines. Therefore, this RNA aptamer is similar to Ade1304 in terms of selectivity, and they might have a similar way of binding.

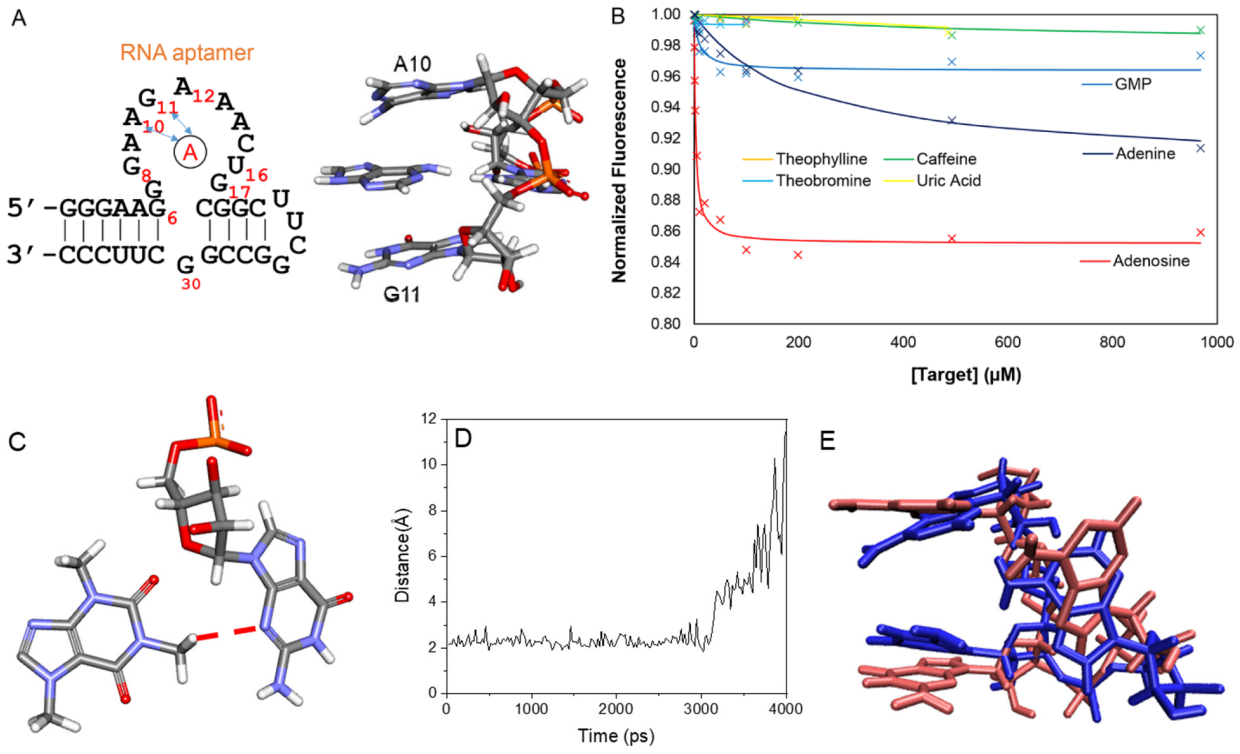

Figure 7. (A) The secondary structure of the RNA aptamer. The strongest binding interactions are from A_{10} and $G_{11,}$ whereas the other nucleotides labeled in red also contributed to binding. The MD simulated structure of the aptamer and adenine as the target, where stacking with A_{10} and G_{11} and hydrogen bonding with G_8 can be seen. This structure is consistent with the NMR structure. (B) ThT binding assays of the RNA ATP aptamer. (C) The binding structure of G_8 and

caffeine in the RNA aptamer. (D) The distance of the two atoms of forming the HB as a function of time. (E) A snapshot of active site of the aptamer in different simulation times. The pink is the initial structure (with caffeine, but caffeine is not shown) and the blue is the final structure (caffeine dissociated).

We then used MD simulations to study this RNA aptamer. We started with an adenine in the active site of the RNA aptamer. The exocyclic amine group is a HB donor and the N1 nitrogen is a HB acceptor, forming two HBs to the unpaired G_8 (Figure 7A). Besides, adenine is stacked between A_{10} and G_{11}. After a standard MD simulation, 2,000 conformations were obtained evenly from a 4 ns MD trajectory. By monitoring the change in the equilibrium structure, one of the two HBs still formed stably during the simulation as its average length is 2.4±0.8 Å whereas the other HB is less stable as its average length is 3±1.3 Å (Figure S3).

We then docked caffeine and chose the lowest energy structure as the initial conformation. After the same procedures as above, caffeine and the aptamer formed one HB (Figure 7C). Following a 4 ns production MD simulation, an interesting phenomenon was revealed. Based on the distance between the two atoms that form the HB (Figure 7D), the HB just exists for 3 ns in the beginning of the MD. Then this bond breaks, dissociating the caffeine. Moreover, the interaction of aptamer and caffeine shows that between 2.5 ns and 3.3 ns, the interaction energy of two molecules increases rapidly (Figure S4). Through an in-depth analysis of the complex structure, the MD conformation reveals that after the caffeine separates from the aptamer, the empty active site of the aptamer becomes smaller (blue) compare to that in the beginning (pink) of the simulation with caffeine bound (Figure 7E). Therefore, for caffeine to bind, it needs to overcome the small size of the pocket, which can impose an additional energy barrier. Hence, the RNA aptamer cannot stably bind caffeine, which is different from DNA aptamer. Finally, we simulated guanine-RNA aptamer complex, and as expected, no stable binding was observed (Figure S5).

The origin of selectivity

Finally, we discuss the origin of selectivity difference for the DNA and RNA aptamers. First, we discuss the structures of the aptamers. In the DNA aptamer, only three bases (G_8, G_9 and A_{10}) directly involved in target binding (Figure 8A). This small binding pocket can only bind part of the target molecule, leading to a lower binding affinity and lower specificity. For the RNA aptamer, based on the NMR structure, many more nucleotides formed a larger binding pocket that can interact with the target AMP more thoroughly (Figure 8B). This better defined binding pocket with more interaction points with the target already implies better affinity and specificity.

Second, based on our MD simulation results, we believe that the flexibility of the binding pockets is another factor. Based on MD simulation, the DNA binding pocket can be in a rigid state even before binding a target molecule due to the base pairing and stacking interactions.[14] On the other hand, the free RNA aptamer pocket has less initial non-canonical base pairing and less base stacking, resulting in a more flexible initial structure. As shown in Figure 8C and Figure 8D, by aligning the structures before and after binding adenine, we discovered that the pocket of the DNA aptamer binding with adenine (blue) is similar to the initial structure (red), but the RNA aptamer active pocket is larger (blue) with the target than before binding the target (white). The reason why these two aptamers show different flexibility is shown in Figure 8E. In the binding pocket of the DNA aptamer, paired bases A_{10} (paired with G_{18}) and G_8 (paired with G_{19}) can stack with caffeine. These two base pairs exist stable during the whole MD simulation. At the same time, caffeine can form hydrogen bond with G_9. This structure can readily accept caffeine binding. In contrast, the bases in the active site of RNA aptamer are free (Figure 8F), and all of them has less initial non-canonical base pairing and less base stacking, which cannot form a stable binding site for caffeine.[14,28] It is thus more difficult for caffeine to achieve an induced-fitting binding.

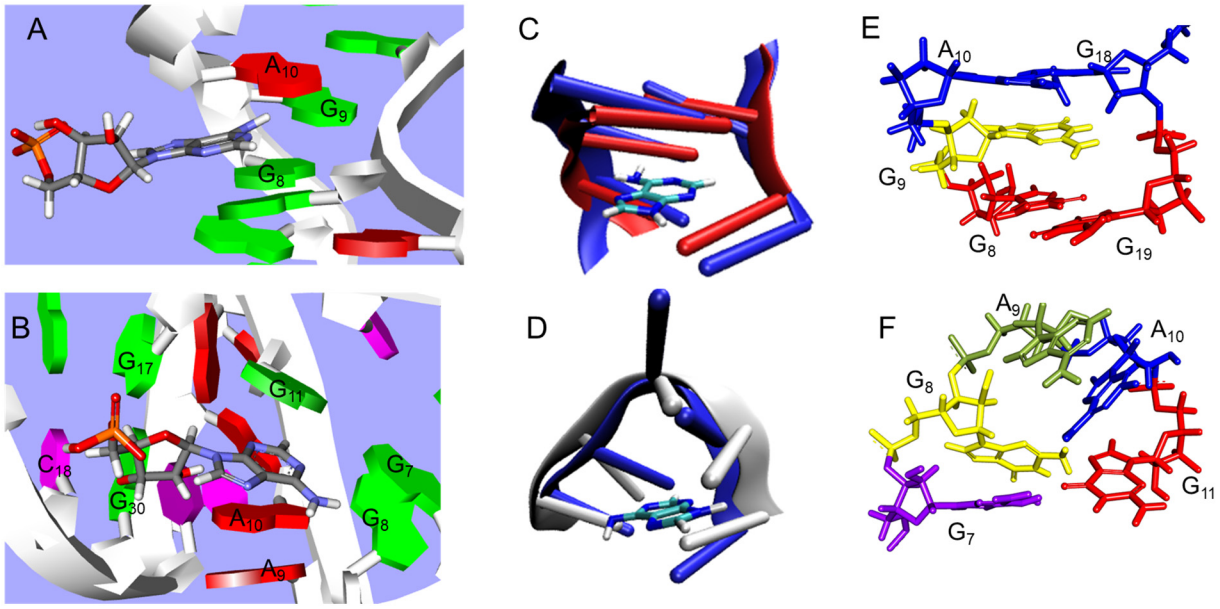

Figure 8. The binding pocket of AMP in (A) the classical DNA aptamer and (B) the RNA aptamer. (C) Aligning the pocket structure of the free DNA aptamer (red) and the DNA aptamer with adenine (blue). (D) Aligning the pocket structure of the free RNA aptamer (white) and the RNA aptamer with adenine (blue). (E) The binding pocket and its paired bases in the DNA aptamer. (F) The binding site in the RNA aptamer.

Conclusions

Aptamers have attracted extensive research interest in the last few decades.[46-49] Aptamers binding to ATP and adenosine have been particularly important since many researchers used them as model systems.[1-3,22] In this work, we performed binding assays for four adenosine/ATP aptamers to a few methylxanthines. The classical DNA aptamer and the newly selected Ade1301 aptamer both showed binding to molecules like caffeine and theophylline. Their binding to caffeine and theophylline was only about 10 to 20 fold weaker than to adenosine. In contrast, the Ade1304 aptamer and the RNA aptamer showed much better selectivity with no observable binding to methylxanthines. Using MD simulations, the origin of selectivity was rationalized. For some analytical applications, potential interference from these molecules need to be considered, especially for those measurements in blood (e.g. caffeine, theophylline may interfere for people drinking coffee and tea). For high selectivity, the Ade1304 aptamer is a better choice for biosensor design.

So far, the classical DNA aptamer appeared in at least six independent selection experiments, three of which used ATP,[3,5,22] and the rest three used adenosine,[22] theophylline[26] and caffeine,[25] respectively. The reason for the occurrence of this aptamer is because of its relative simple binding requirements and only 12 conserved nucleotides are required. To obtain new aptamers and avoid the recurrence of this motif, low target concentrations and negative selections are recommended.[22,50]

Acknowledgements

We thank Ms. Natasha Marie Evans for assistance with in vitro transcription to obtain the RNA aptamer. Funding for this work was from a Mitacs Accelerate grant and from the Natural Sciences and Engineering Research Council of Canada (NSERC).

Supporting Information.

Fraction of sequences containing the classical adenosine aptamer in caffeine and theophylline selections; additional MD simulation data and methods for MD simulations (PDF)

References

1. Li, Y., and Liu, J. (2020) Aptamer-Based Strategies for Recognizing Adenine, Adenosine, ATP and Related Compounds, *Analyst 145*, 6753-6768.
2. Sassanfar, M., and Szostak, J. W. (1993) An RNA Motif That Binds ATP, *Nature 364*, 550-553.

3. Huizenga, D. E., and Szostak, J. W. (1995) A DNA Aptamer That Binds Adenosine and ATP, *Biochemistry 34*, 656-665.
4. Zhang, Z., Oni, O., and Liu, J. (2017) New Insights into a Classic Aptamer: Binding Sites, Cooperativity and More Sensitive Adenosine Detection, *Nucleic Acids Res. 45*, 7593-7601.
5. Nutiu, R., and Li, Y. (2005) In Vitro Selection of Structure-Switching Signaling Aptamers, *Angew. Chem. Int. Ed. 44*, 1061-1065.
6. Zheng, D., Seferos, D. S., Giljohann, D. A., Patel, P. C., and Mirkin, C. A. (2009) Aptamer Nano-Flares for Molecular Detection in Living Cells, *Nano Lett. 9*, 3258-3261.
7. Li, L.-L., Ge, P., Selvin, P. R., and Lu, Y. (2012) Direct Detection of Adenosine in Undiluted Serum Using a Luminescent Aptamer Sensor Attached to a Terbium Complex, *Anal. Chem. 84*, 7852-7856.
8. Nutiu, R., and Li, Y. (2003) Structure-Switching Signaling Aptamers, *J. Am. Chem. Soc. 125*, 4771-4778.
9. Peng, P., Shi, L. L., Wang, H. H., and Li, T. (2017) A DNA Nanoswitch-Controlled Reversible Nanosensor, *Nucleic Acids Res. 45*, 541-546.
10. Zhao, J., Gao, J. H., Xue, W. T., Di, Z. H., Xing, H., Lu, Y., and Li, L. L. (2018) Upconversion Luminescence-Activated DNA Nanodevice for Atp Sensing in Living Cells, *J. Am. Chem. Soc. 140*, 578-581.
11. Mariottini, D., Idili, A., Nijenhuis, M. A. D., de Greef, T. F. A., and Ricci, F. (2018) DNA-Based Nanodevices Controlled by Purely Entropic Linker Domains, *J. Am. Chem. Soc. 140*, 14725-14734.
12. Zhao, D., Chang, D. R., Zhang, Q., Chang, Y. Y., Liu, B., Sun, C. S., Li, Z. P., Dong, C., Liu, M., and Li, Y. F. (2021) Rapid and Specific Imaging of Extracellular Signaling Molecule Adenosine Triphosphate with a Self-Phosphorylating DNAzyme, *J. Am. Chem. Soc. 143*, 15084-15090.
13. Slavkovic, S., Eisen, S. R., and Johnson, P. E. (2020) Designed Alteration of Binding Affinity in Structure-Switching Aptamers through the Use of Dangling Nucleotides, *Biochemistry 59*, 663-670.
14. Xie, Y. C., Eriksson, L. A., and Zhang, R. B. (2020) Molecular Dynamics Study of the Recognition of ATP by Nucleic Acid Aptamers, *Nucleic Acids Res. 48*, 6471-6480.
15. Xia, T., Yuan, J., and Fang, X. (2013) Conformational Dynamics of an Atp-Binding DNA Aptamer: A Single-Molecule Study, *J. Phys. Chem. B 117*, 14994-15003.
16. Lin, C. H., and Patel, D. J. (1997) Structural Basis of DNA Folding and Recognition in an AMP-DNA Aptamer Complex: Distinct Architectures but Common Recognition Motifs for DNA and RNA Aptamers Complexed to Amp, *Chem.Biol. 4*, 817-832.
17. Slavkovic, S., Zhu, Y., Churcher, Z. R., Shoara, A. A., Johnson, A. E., and Johnson, P. E. (2020) Thermodynamic Analysis of Cooperative Ligand Binding by the ATP-Binding DNA Aptamer Indicates a Population-Shift Binding Mechanism, *Sci. Rep. 10*, 18944.
18. Barbu, M., and Stojanovic, M. N. (2012) A Fresh Look at Adenosine-Binding DNA Motifs, *ChemBioChem 13*, 658-660.
19. Nakatsuka, N., Yang, K.-A., Abendroth, J. M., Cheung, K. M., Xu, X., Yang, H., Zhao, C., Zhu, B., Rim, Y. S., Yang, Y., Weiss, P. S., Stojanović, M. N., and Andrews, A. M. (2018)

Aptamer–Field-Effect Transistors Overcome Debye Length Limitations for Small-Molecule Sensing, *Science 362*, 319-324.
20. Yang, K.-A., Chun, H., Zhang, Y., Pecic, S., Nakatsuka, N., Andrews, A. M., Worgall, T. S., and Stojanovic, M. N. (2017) High-Affinity Nucleic-Acid-Based Receptors for Steroids, *ACS Chem. Biol. 12*, 3103-3112.
21. Huang, P.-J. J., and Liu, J. (2023) Simultaneous Detection of L-Lactate and D-Glucose Using DNA Aptamers in Human Blood Serum, *Angew. Chem. Int. Ed. 62*, e202212879.
22. Ding, Y., and Liu, J. (2023) Pushing Adenosine and ATP SELEX for DNA Aptamers with Nanomolar Affinity, *J. Am. Chem. Soc. 145*, 7540–7547.
23. Jenison, R. D., Gill, S. C., Pardi, A., and Polisky, B. (1994) High-Resolution Molecular Discrimination by RNA, *Science 263*, 1425-1429.
24. Wrist, A., Sun, W., and Summers, R. M. (2020) The Theophylline Aptamer: 25 Years as an Important Tool in Cellular Engineering Research, *ACS Synth. Biol. 9*, 682-697.
25. Huang, P.-J. J., and Liu, J. (2022) Selection of Aptamers for Sensing Caffeine and Discrimination of Its Three Single Demethylated Analog, *Anal. Chem. 94*, 3142–3149.
26. Huang, P.-J. J., and Liu, J. (2022) A DNA Aptamer for Theophylline with Ultrahigh Selectivity Reminiscent of the Classic RNA Aptamer, *ACS Chem. Biol. 17*, 2121–2129.
27. Perez Tobia, J., Huang, P.-J. J., Ding, Y., Saran Narayan, R., Narayan, A., and Liu, J. (2023) Machine Learning Directed Aptamer Search from Conserved Primary Sequences and Secondary Structures, *ACS Synth. Biol. 12*, 186–195.
28. Dieckmann, T., Suzuki, E., Nakamura, G. K., and Feigon, J. (1996) Solution Structure of an Atp-Binding RNA Aptamer Reveals a Novel Fold, *RNA 2*, 628-640.
29. Humphrey, W., Dalke, A., and Schulten, K. (1996) VMD: Visual Molecular Dynamics, *J. Mol. Graph. 14*, 33-38.
30. Phillips, J. C., Braun, R., Wang, W., Gumbart, J., Tajkhorshid, E., Villa, E., Chipot, C., Skeel, R. D., Kalé, L., and Schulten, K. (2005) Scalable Molecular Dynamics with NAMD, *J. Comput. Chem. 26*, 1781-1802.
31. Foloppe, N., and MacKerell, J., Alexander D. (2000) All-Atom Empirical Force Field for Nucleic Acids: I. Parameter Optimization Based on Small Molecule and Condensed Phase Macromolecular Target Data, *J. Comput. Chem. 21*, 86-104.
32. Vanommeslaeghe, K., Hatcher, E., Acharya, C., Kundu, S., Zhong, S., Shim, J., Darian, E., Guvench, O., Lopes, P., Vorobyov, I., and Mackerell Jr., A. D. (2010) Charmm General Force Field: A Force Field for Drug-Like Molecules Compatible with the Charmm All-Atom Additive Biological Force Fields, *J. Comput. Chem. 31*, 671-690.
33. Zoete, V., Cuendet, M. A., Grosdidier, A., and Michielin, O. (2011) Swissparam: A Fast Force Field Generation Tool for Small Organic Molecules, *J. Comput. Chem. 32*, 2359-2368.
34. Miyamoto, S., and Kollman, P. A. (1992) Settle: An Analytical Version of the Shake and Rattle Algorithm for Rigid Water Models, *J. Comput. Chem. 13*, 952-962.
35. Darden, T., York, D., and Pedersen, L. (1993) Particle Mesh Ewald: An N·Log(N) Method for Ewald Sums in Large Systems, *J. Chem. Phys. 98*, 10089-10092.
36. Feller, S. E., Zhang, Y., Pastor, R. W., and Brooks, B. R. (1995) Constant Pressure Molecular Dynamics Simulation: The Langevin Piston Method, *J. Chem. Phys. 103*, 4613-4621.

37. Martyna, G. J., Tobias, D. J., and Klein, M. L. (1994) Constant Pressure Molecular Dynamics Algorithms, *J. Chem. Phys. 101*, 4177-4189.
38. Yeasmin Khusbu, F., Zhou, X., Chen, H., Ma, C., and Wang, K. (2018) Thioflavin T as a Fluorescence Probe for Biosensing Applications, *TrAC, Trends Anal. Chem. 109*, 1-18.
39. Zhang, F., Huang, P.-J. J., and Liu, J. (2020) Sensing Adenosine and Atp by Aptamers and Gold Nanoparticles: Opposite Trends of Color Change from Domination of Target Adsorption Instead of Aptamer Binding, *ACS Sensors 5*, 2885–2893.
40. Zhang, H., Li, A. Z., and Liu, J. (2023) Surfactant-Assisted Label-Free Fluorescent Aptamer Biosensors and Binding Assays, *Biosensors 13*, 434.
41. Canoura, J., Yu, H., Alkhamis, O., Roncancio, D., Farhana, R., and Xiao, Y. (2021) Accelerating Post-Selex Aptamer Engineering Using Exonuclease Digestion, *J. Am. Chem. Soc. 143*, 805-816.
42. Biniuri, Y., Albada, B., and Willner, I. (2018) Probing ATP/ATP-Aptamer or ATP-Aptamer Mutant Complexes by Microscale Thermophoresis and Molecular Dynamics Simulations: Discovery of an ATP-Aptamer Sequence of Superior Binding Properties, *J. Phys. Chem. B 122*, 9102-9109.
43. Slavkovic, S., and Johnson, P. E. (2018) Isothermal Titration Calorimetry Studies of Aptamer-Small Molecule Interactions: Practicalities and Pitfalls, *Aptamers 2*, 45-51.
44. Turnbull, W. B., and Daranas, A. H. (2003) On the Value of C: Can Low Affinity Systems Be Studied by Isothermal Titration Calorimetry?, *J. Am. Chem. Soc. 125*, 14859-14866.
45. Jiang, F., Kumar, R. A., Jones, R. A., and Patel, D. J. (1996) Structural Basis of RNA Folding and Recognition in an AMP-RNA Aptamer Complex, *Nature 382*, 183-186.
46. Famulok, M., Hartig, J. S., and Mayer, G. (2007) Functional Aptamers and Aptazymes in Biotechnology, Diagnostics, and Therapy., *Chem. Rev. 107*, 3715-3743.
47. Wu, L., Wang, Y., Xu, X., Liu, Y., Lin, B., Zhang, M., Zhang, J., Wan, S., Yang, C., and Tan, W. (2021) Aptamer-Based Detection of Circulating Targets for Precision Medicine, *Chem. Rev. 121*, 12035–12105.
48. McConnell, E. M., Nguyen, J., and Li, Y. (2020) Aptamer-Based Biosensors for Environmental Monitoring, *Front. Chem. 8*, 434.
49. Zhao, Y., Yavari, K., and Liu, J. (2022) Critical Evaluation of Aptamer Binding for Biosensor Designs, *TrAC, Trends Anal. Chem. 146*, 116480.
50. Alkhamis, O., and Xiao, Y. (2023) Systematic Study of in Vitro Selection Stringency Reveals How to Enrich High-Affinity Aptamers, *J. Am. Chem. Soc. 145*, 194-206.

For TOC Graphics Only